

Zhao, X.B., Seltnann, R., Xue, C.J., and Sun, Q., 2024, Orogenic cyclicity and episodic tectono-magmatic processes in the formation of the Paleozoic northern Yili magmatic arc, Central Asian Orogenic Belt: GSA Bulletin, <https://doi.org/10.1130/B37192.1>.

Supplemental Material

Supplemental Text S1. Analytical methods

Supplemental Text S2. Data filtered methods

Figure S1. Photomicrographs of the intrusive lithologies of five plutons in the northern Yili block.

Figure S2. (a, h, o) Alteration box plot, after Large et al. (2001). (b-g, i-n, p-u) Variation diagrams of highly mobile elements with loss-on-ignition (LOI) for magmatic rock samples in the north Yili Block.

Figure S3. (a-c) Zr/Hf vs. Y/Ho diagram (modified after Bau, 1996), CHARAC (CHArge-and-Radius-Controlled) field represents common magmatic rocks crystallized from pure silica melt systems. (d-f) Nb vs. Nb/Ta diagram (modified after Ballouard et al., 2016), Nb/Ta < 5 areas represent the feature of highly fractionated magmatic rocks.

Table S1. Zircon LA-ICP-MS U-Pb isotopic compositions of the investigated granitic intrusion in the northern Yili magmatic arc.

Table S2. Whole-rock major (wt.%) and trace (ppm) element compositions of the investigated granitic intrusion in the northern Yili magmatic arc.

Table S3. Whole-rock Sr-Nd isotopic compositions of the investigated granitic intrusion in the northern Yili magmatic arc.

Table S4. Zircons Hf isotopic compositions of the investigated granitic intrusion in the northern Yili magmatic arc.

Table S5. Zircon trace element compositions (in ppm) of the investigated granitic intrusion in the northern Yili magmatic arc.

Table S6. Compilation of zircon U-Pb ages from the Paleozoic magmatic rocks of northern Yili magmatic arc.

Table S7. Compilation whole-rock major (wt.%) and trace (ppm) element compositions from the Paleozoic magmatic rocks in the northern Yili magmatic arc.

Table S8. Compilation whole-rock Sr-Nd isotopic compositions from the Paleozoic magmatic rocks of northern Yili and northern Balkhash area of the Balkhash-Yili arc.

Table S9. Compilation of zircons Hf isotopic compositions from the Paleozoic magmatic rocks of northern Yili and northern Balkhash area in the Balkhash-Yili arc.

Table S10. Calculated whole-rock crystallization temperatures from selected magmatic rocks in the northern Yili magmatic arc.

Table S11. Calculated crustal thickness from selected magmatic rocks in the northern Yili magmatic arc.

Supplemental Text S1: Analytical methods

Zircon U-Pb dating and trace element geochemistry

Zircon grains were separated from the samples using conventional crushing, heavy liquid, and magnetic separation techniques before the separates were purified by handpicking under a binocular microscope at the Langfang Yantuo Geological Service, Hebei Province, China. The handpicked zircons were mounted in epoxy resin and polished to expose grain centers. Using a combination of cathodoluminescence (CL) and optical microscopy, the clearest, least fractured rims of the zircon crystals were selected as suitable targets for laser ablation analyses. Agilent 7500a ICP-MS equipped with a 193 nm laser, housed at the State Key Laboratory of Geological Processes and Mineral Resources, China University of Geosciences (Wuhan), was used to measure the U-Pb age of zircons. Zircon 91500 was used as external standard for age calibration and the NIST SRM 610 silicate glass was applied for the instrument optimization. The crater diameter was 30 μm during the analyses. The ICPMSDataCal and Isoplot programs were used for data reduction. Correction for common Pb was made following Anderson (2002). Errors on individual analyses by LA-ICP-MS are quoted at the 1σ level, while errors on pooled ages are quoted at the 95% (2σ) confidence level. Zircon trace-element analysis are synchronous with U-Pb dating. The NIST 612 was conducted as standard sample to correct for mass bias drift. Silicon concentration was applied for elemental calibration. Accuracy for selected elements is within 10%.

Whole-rock geochemistry

Samples for whole-rock analysis were cleaned, and altered material removed, prior to crushing in an agate mill to pass ~ 200 mesh. The whole-rock major and trace element abundances were obtained at the State Key Laboratory of Geological Processes and Mineral Resources, China University of Geosciences, Wuhan, China. Major elements were analyzed by X-ray fluorescence (XRF) using a Rigaku RIX 2100 spectrometer. Trace elements were determined by ICP-MS after acid digestion of samples in Teflon bombs using an Agilent 7500a equipped with a shield torch. Analytical uncertainties are between 1% and 3%, and analyses of the BHVO-1 (basalt), BCR-2 (basalt), and AGV-1 (andesite) standards indicate that the analytical precision for major elements was better than 5% and for trace elements generally better than 10%.

Whole-rock Sr and Nd isotopes

The whole-rock Nd isotope of samples was analyzed in the state key laboratory Geological Process and Mineral Resources, School of Earth Sciences and Mineral Resources, China University of Geosciences Beijing (CUGB). Sample powders (50–100 mg) were dissolved in HF-HNO₃-HCl-HClO₄ completely. Nd was purified by LN resin and HCl, then after the AG50-X12 resin. The Nd isotope was corrected by $^{146}\text{Nd}/^{144}\text{Nd} = 0.7219$. The purified Nd was dissolved in 3% HNO₃ for isotope analysis on the TIMS. The geology standard of BHVO-2 and GSP-2 of $^{143}\text{Nd}/^{144}\text{Nd}$ is $= 0.512994 \pm 9$ (2σ) and 0.511335 ± 11 (2σ), respectively, for this study. Alfa Nd (An ultrapure single elemental standard solution from the Alfa Aesar A Johnson Matthey Company of the USA) was analyzed as the in-house reference. The Alfa Nd for this study is Alfa Nd $^{143}\text{Nd}/^{144}\text{Nd} = 0.512427 \pm 10$ (2σ), which is similar to the long-term measured values in this clean lab for it is Alfa Nd $^{143}\text{Nd}/^{144}\text{Nd} = 0.512423 \pm 24$ (2σ , $n = 58$).

Zircon Lu-Hf isotope

In-situ zircon Hf isotope analyses were undertaken by MC-ICP-MS (Neptune Plus) equipped with a 193 nm ArF excimer laser ablation system at the State Key Laboratory of Geological Processes and Mineral Resources, China University of Geosciences. A simple Y junction downstream from the sample cell was used to add small amounts of nitrogen (4 ml min⁻¹) to the argon gas; the addition of nitrogen in combination with the use of a newly designed X skimmer and Jet sample cones within the Neptune Plus instrument improved the signal intensities of Hf, Yb, and Lu by factors of 5.3, 4.0, and 2.4, respectively, when compared with standard arrangements. All data were acquired using a single spot ablation mode and a 44 µm spot size. Each measurement consisted of 20 s of background signal acquisition followed by 50 s of ablation signal acquisition. Details of the operating conditions for the laser ablation system and the MC-ICP-MS instrument, and details of the analytical methods used during this study, are given in Hu et al. (2012).

Supplemental Text S2. Data filtered methods

Evaluating of alteration affect

Generally, magmatic rocks with relatively high loss-on-ignition (LOI) values (>5%) imply that they may have undergone various processes of hydrothermal alteration. The alteration processes would alter the compositions of major and trace elements. In the cases, we select some magmatic rocks (most are basaltic volcanic rocks) to evaluate the effect of hydrothermal alteration.

In the figure 1a, some samples of andesite (samples: TS35-4-TS35-7; WT809-WT825) locate or close to the alteration areas. In the figure 1b-1g, TS35-4-TS35-7 samples show obviously covariant variations that demonstrates these samples experienced later hydrothermal alteration. Whereas, WT809-WT825 samples exhibit few correlations that implies they were not affected by post-magmatic alteration (Fig. 1b-g). In the figure 1h, most of selected samples (BG7-BG9; H-801-1-H-nx-4; WXT721-P201; H-009-1-H-309-15) plot in or close to the alteration areas. However, most of these samples (except BG7-BG9) present weak correlations between highly mobile elements and LOI (Figure. 1i-n), which suggests that they not underwent significant alteration processes. In the figure 1o, basaltic volcanic rocks (samples: KK1-10-QB-2C; 04XJ-327-04XJ-340; 06XJ112-1-06XJ114-2) locate in the alteration areas. A few samples (04XJ-327-04XJ-340) exhibit strong correlations between highly mobile elements and LOI that indicates that they were affected by alteration, whereas most of samples have not obvious alteration features (Figure. 1p-1u).

Therefore, we exclude probable alteration samples (i.e., TS35-4-TS35-7; BG7-BG8; 04XJ329; 04XJ340) in this study.

Filtration of highly fractionated magmatic rocks

Highly fractionated magmatic rocks (SiO₂ > 70 wt %) generally experience complex processes of magmatic evolution, which result in their variable compositions of major and trace elements and controversial petrogenetic mechanism (Wu et al., 2017). In this case, we not use them to discuss the magmatic evolution of the North Yili belt in this study.

Many pioneer works have recognized some distinct characteristic for identifying highly fractionated magmatic rocks (e.g., Nb/Ta < 5, Ballouard et al., 2016; Zr/Hf: < 26 and > 46, Y/Ho: < 24 and > 34, Bau, 1996). In the Zr/Hf vs. Y/Ho diagram, many 380-350 Ma and 300-260 Ma magmatic rocks show relatively low Zr/Hf ratios, which indicated they underwent highly fractionated magmatic processes (Fig. 2a-c). Also, some 320-300 Ma and 300-260 Ma magmatic

rocks exhibit extremely low Nb/Ta ratios suggest that they experienced similar highly fractionated evolution (Fig. 2d-f). As above-mentioned evidences, we recognize some highly fractionated magmatic rocks and preclude them for this discussion (excluded samples in supplementary Table S6).

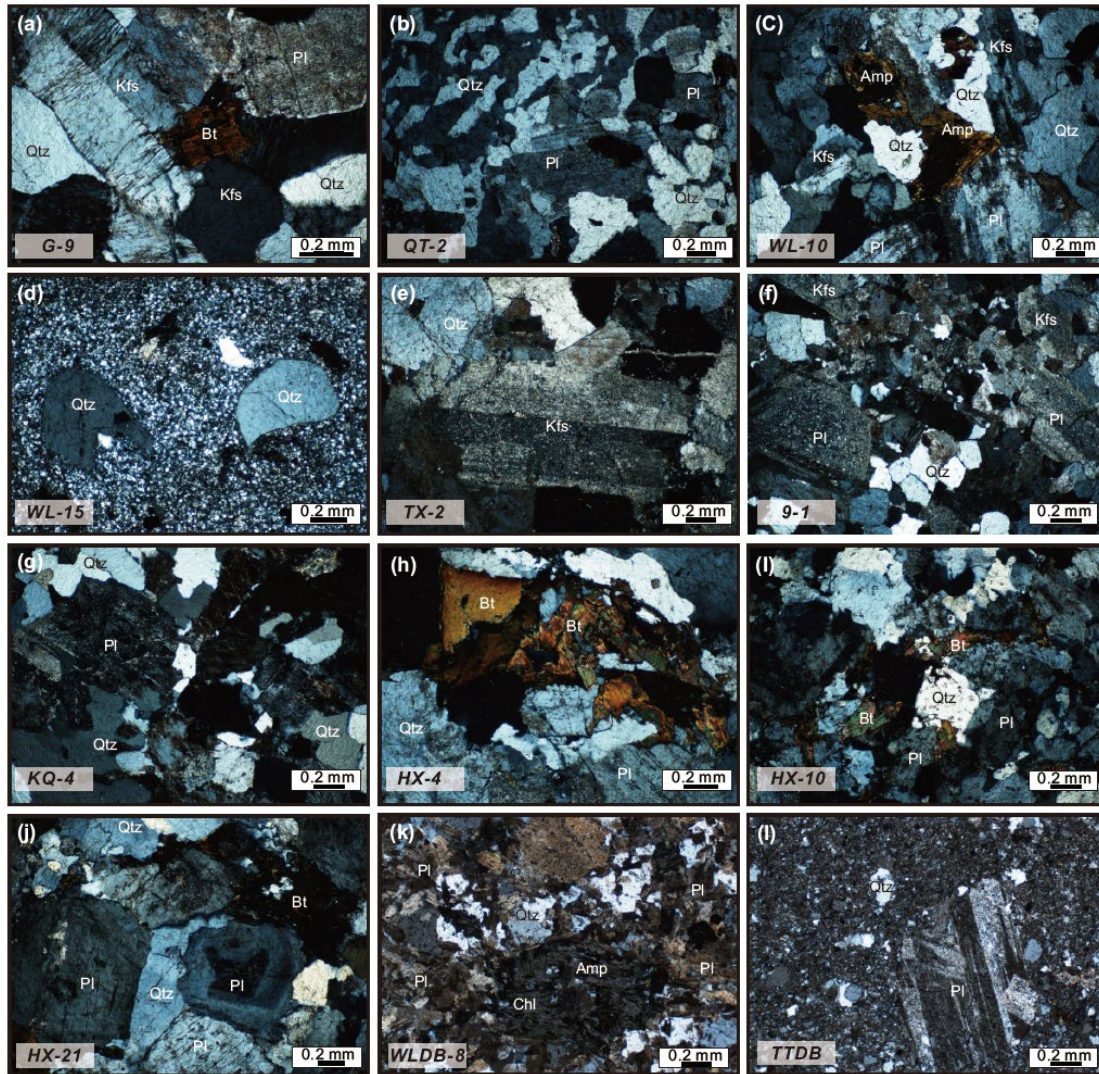
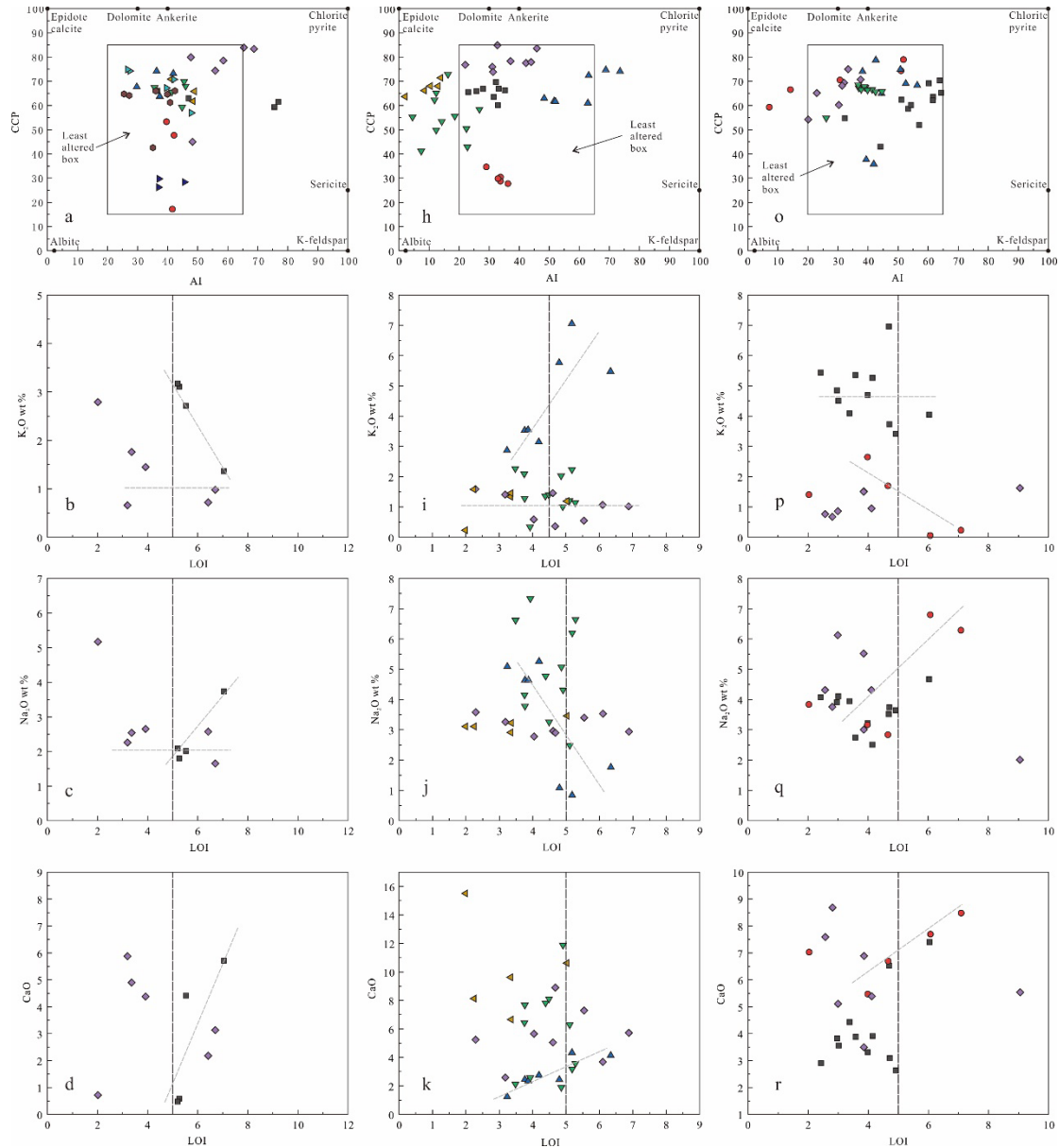


Figure S1. Photomicrographs of the intrusive lithologies of five plutons in the northern Yili block. All the photomicrographs are under crossed nicols. Guozigou pluton: (a) monzogranite showing a medium to fine grained texture and composed mostly of K-feldspar, plagioclase, quartz and biotite; (b) monzogranite locally showing quartz irregularly distributed in the plagioclase; Wulanbulark pluton: (c) quartz diorite composed of K-feldspar, plagioclase, quartz and amphibole; (d) granite porphyry showing a porphyritic texture; Kekeqiao-kenxia pluton: (e) K-feldspar granite showing a medium to coarse grained texture with a characteristic K-feldspar Carlsbad twin; (f, g) monzogranite composed mainly of K-feldspar, plagioclase and quartz, and a related variation of the K-feldspar component; Haxilegen pluton: (h, i) biotite with a dark yellow interference color distributed between plagioclase and quartz, and showing variable grain size and abundance; (j) granodiorite containing plagioclase, quartz and biotite with local plagioclase showing a characteristic oscillatory zoning; Wulangdaban-Tetiedaban pluton:

(k) granite porphyry showing a porphyritic texture with phenocrysts of plagioclase, quartz and amphibole; (l) albite porphyry exhibiting albite and minor quartz phenocrysts in the matrix with an obvious albite twin.



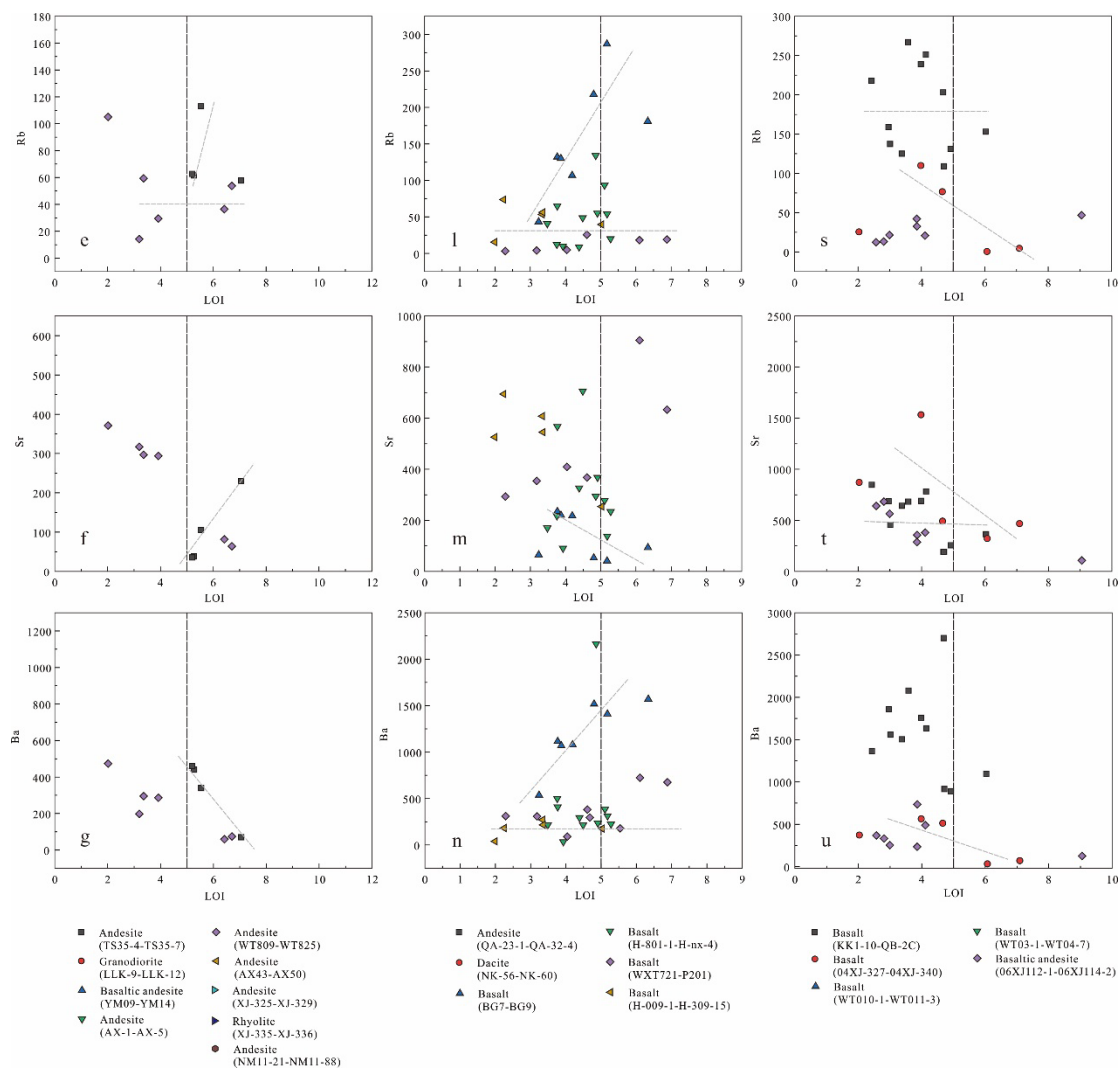


Figure S2. (a, h, o) Alteration box plot, after Large et al. (2001). (b-g, i-n, p-u) Variation diagrams of highly mobile elements with loss-on-ignition (LOI) for magmatic rock samples in the north Yili Block. The data of these samples are from Supplementary Table S6. AI (Ishikawa Alteration Index) = $100 \times (K_2O + MgO) / (K_2O + MgO + Na_2O + CaO)$, CCP (Chlorite-carbonate-pyrite index) = $100 \times (MgO + FeO^T) / (MgO + FeO^T + Na_2O + K_2O)$.

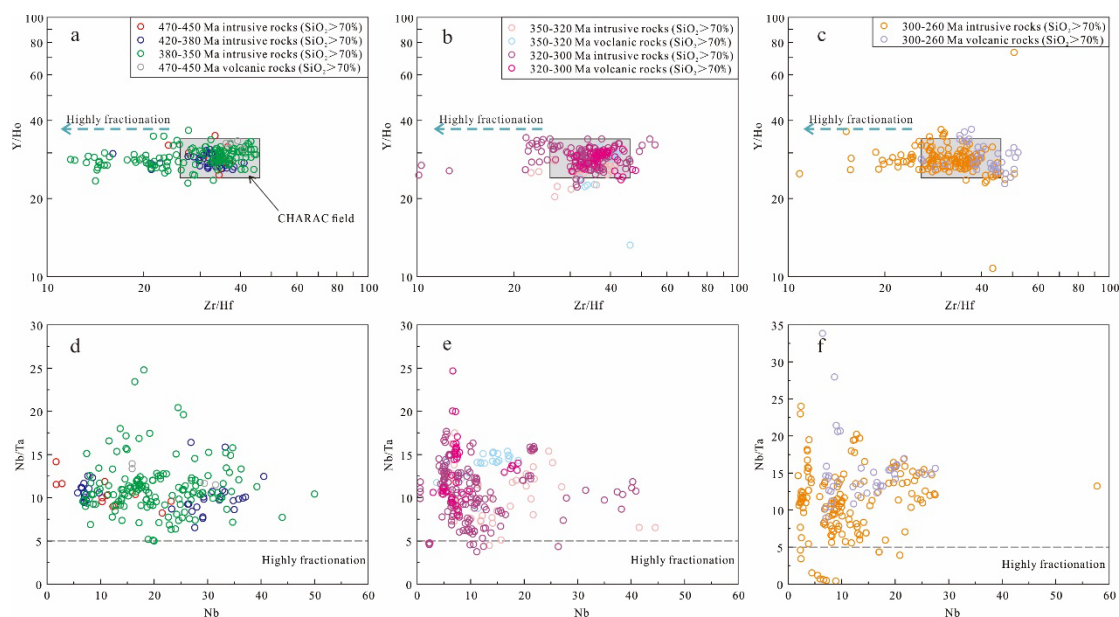


Figure S3. (a-c) Zr/Hf vs. Y/Ho diagram (modified after Bau, 1996), CHARAC (CHARGE-and-Radius-Controlled) field represents common magmatic rocks crystallized from pure silica melt systems. (d-f) Nb vs. Nb/Ta diagram (modified after Ballouard et al., 2016), Nb/Ta < 5 areas represent the feature of highly fractionated magmatic rocks.

Reference:

- Andersen, T., 2002. Correction of common lead in U-Pb analyses that do not report ²⁰⁴Pb. *Chemical Geology* 192, 59–79.
- Ballouard, C., Poujol, M., Boulvais, P., Branquet, Y., Tartèse, R., Vigneresse, J.L., 2016. Nb-Ta fractionation in peraluminous granites: A marker of the magmatic-hydrothermal transition. *Geology* 44, 231–23.
- Bau, M., 1996. Controls on the fractionation of isovalent trace elements in magmatic and aqueous systems: Evidence from Y/Ho, Zr/Hf, and lanthanide tetrad effect. *Contributions to Mineralogy and Petrology* 123, 323–33.
- Hu, Z., Liu, Y., Gao, S., Liu, W., Zhang, W., Tong, X., Lin, L., Zong, K., Li, M., Chen, H., Zhou, L., Yang, L., 2012. Improved in situ Hf isotope ratio analysis of zircon using newly designed X skimmer cone and jet sample cone in combination with the addition of nitrogen by laser ablation multiple collector ICP-MS. *Journal of Analytical Atomic Spectrometry* 27(9), 1391–1399.
- Large, R.R., Gemmell, B., Paulick, H., 2001. The Alteration box plot: A simple approach to understanding the relationship between alteration mineralogy and lithogeochemistry associated with volcanic-hosted massive sulfide deposits. *Economic Geology* 96, 957–971.
- Wu, F.Y., Liu, X.C., Ji, W.Q., Wang, J.M., Yang, L., 2017. Highly fractionated granites: Recognition and research. *Science China Earth Sciences* 60, 1201–1219.